



Effects of Bi doping on thermoelectric properties of Cu₂Se materials by high-pressure synthesis

Lisha Xue¹ · Weixia Shen² · Zhuangfei Zhang² · Chao Fang² · Yuewen Zhang² · Xiaopeng Jia²

Received: 30 September 2020 / Accepted: 21 December 2020 / Published online: 7 January 2021
© The Author(s), under exclusive licence to Springer-Verlag GmbH, DE part of Springer Nature 2021

Abstract

Motivated by prototypes that the heavy-element doping can effectively tune carrier and phonon transport behavior, we studied the influence of Bi doping on the thermoelectric properties of Cu₂Se synthesized by high-pressure and high-temperature technique. With the increased Bi contents, the carrier mobility of Bi_xCu₂Se samples distinctly decreased, while the Seebeck coefficient and electrical resistivity increased. The Bi_xCu₂Se samples exhibited multiple microstructures including abundant grain boundaries, micropores and lattice defects. Various phonon scattering mechanisms generated relatively low lattice thermal conductivity below 0.55 Wm⁻¹ K⁻¹ for all Cu₂Se-based samples. The lattice thermal conductivity of Cu₂Se-based samples increased after Bi doping due to reduced degree of disorder of Cu⁺ ions, which weakened phonon scattering. Due to the significantly reduced thermal conductivity, a peak zT value of 1.57 at 873 K was obtained for Bi_{0.005}Cu₂Se sample, which was 25% higher than that of pristine Cu₂Se (zT ~ 1.25). This work indicates the potential of heavy-element doping in boosting performance for liquid-like thermoelectrics.

Keywords High pressure · Thermoelectric property · Cu₂Se · Bi doping

1 Introduction

Thermoelectric (TE) materials can directly convert between temperature difference and electricity, which offers a feasibility to solve energy crisis and environmental pollution [1–5]. The TE performance is determined by zT value, $zT = S^2\sigma T/\kappa$, where S, σ , T and κ are the Seebeck coefficient, electrical conductivity, absolute temperature and the thermal conductivity, respectively. Boosting the zT value can effectively improve TE conversion efficiency. Some TE materials have zT values in excess of 2, such as PbTe alloyed with CaTe and BaTe achieved a maximum zT ~ 2.2 [6] and single-crystal SnSe exhibited a maximum zT ~ 2.6 [7]. However, the toxicity and scarcity of Pb/Te elements and anisotropy of SnSe hinder the large-scale development of such materials.

In recent years, Cu₂Se-based materials are widely studied because of low-toxicity, cheapness and earth abundance. Meanwhile, as a phonon-liquid electron-crystal (PLEC) material, Cu₂Se materials exhibit potentially high-TE performance due to the relatively low thermal conductivity [8]. Cu₂Se exhibits two typical crystal structures, the low-temperature α -phase Cu₂Se (monoclinic, C2/c) below 400 K and the high-temperature β -phase Cu₂Se (cubic, Fm-3 m) above 400 K [9, 10]. Cu⁺ ions in low-temperature phase are static in the face-centered cubic sublattice of Se, while they have high mobility in high-temperature phase showing superionic feature. The ultra-low lattice thermal conductivity is a key factor for increasing the overall zT value. The peak zT of ~ 2.4 at 1000 K and zT of ~ 2.6 at 850 K were achieved in Cu₂Se/0.75wt% CNT composites and (Cu₂Se)_{0.99}(CuInSe₂)_{0.01}, respectively [11, 12]. Doping is one of the most effective method to optimize carrier concentration and enhance the TE properties [13]. Moreover, dopants can enhance the phonon scattering as lattice/interface distortions to decrease the thermal conductivity [14]. Many researches have been reported such as Ag [15], Li [16], Na [17], S [18], Sn [19], Te [20], CNTs [11] and SiC [21]. Heavy-element dopants have attracted our attention, which means that doping heavy-element is a feasible

✉ Yuewen Zhang
zhangyw@zzu.edu.cn

¹ College of Science, Henan University of Engineering, Zhengzhou 451191, China

² Key Laboratory of Material Physics of the Ministry of Education, School of Physics and Microelectronics, Zhengzhou University, Zhengzhou 450052, China

method to enhance the complexity of the system. Recently, Liao et al. reported that Bi doping into α -Cu₂Se generated enhanced TE properties at near room temperature [22].

Generally, chemical doping is realized by wet-chemical method, ball milling or melting-annealing method to obtain the Cu₂Se powder, and then pressed into blocks by hot press sintering or spark plasma sintering (SPS). However, such processes usually take more than tens of hours or even several days to achieve the final samples, which is time consuming. In recent years, high-pressure technology has been utilized in synthesizing TE materials. The advantages of high-pressure technology have been exhibited in TE properties tuning in Bi₂Te₃ [23], PbTe [24], SnSe [25], etc. Previously, the high-pressure and high-temperature (HPHT) method was developed to directly fabricate Cu₂Se bulk materials from elements powders in half an hour [26, 27]. HPHT technology can effectively modulate the electronic band structure and the microstructures. Besides, the enhanced TE properties of Cu₂Se are retained even when pressure is released.

In this study, Bi_xCu₂Se ($x=0, 0.005, 0.01, 0.02$ and 0.03) materials were synthesized by HPHT method. The effects of Bi doping on the morphology, microstructure and TE transport properties of Cu₂Se were systematically investigated. Bi doping could increase the carrier concentration and also increase lattice thermal conductivity. Eventually, a maximum zT of 1.57 at 873 K was achieved for Bi_{0.005}Cu₂Se sample.

2 Experimental section

2.1 Synthesis

Polycrystalline Bi_xCu₂Se ($x=0, 0.005, 0.01, 0.02,$ and 0.03) bulk samples were prepared by high-pressure and high-temperature technique with element powders of Cu (99.9%, Aladdin), Se (99.99%, Aladdin) and Bi (99.99%, Aladdin) as raw materials. The sample synthesis was divided into two processes. (1) High-pressure synthesis process. The Cu, Se and Bi powders were weighed in stoichiometric proportion and grounded uniformly in Ar-filled glove box. The mixed powders were cold-pressed into disks (Φ 10 mm). The disks were assembled into the synthetic chamber and placed in cubic anvil high-pressure apparatus (BT-320) to perform HPHT synthesis. High pressure was generated by the compression of hydraulic-driven WC anvils and high temperature was produced by electric current heating graphite crucible in the synthetic chamber. The pressure was calculated by a calibration curve based on the known pressure-induced phase transitions and the temperature was measured by Pt-Rh30%/Pt-Rh6% thermocouple. As the pressure was maintained at 3 GPa during the whole synthesis process,

the temperature was kept at 500 °C for 15 min, and raised to 1000 °C in 1 min and kept for another 15 min. The pressure was gradually released to ambient condition after the temperature was quenched to room temperature. (2) High-pressure sintering process. The as-prepared Bi_xCu₂Se bulks were annealed at 700 °C for 12 h in vacuum. After that, a small amount of deposited copper could be removed from the surfaces. The disks were crushed into powder and then sintered to densify the samples under the pressure of 3 GPa and the temperature of 800 °C for 5 min. Figure 1a shows the schematic of the manufacturing process of the Bi-doped Cu₂Se samples.

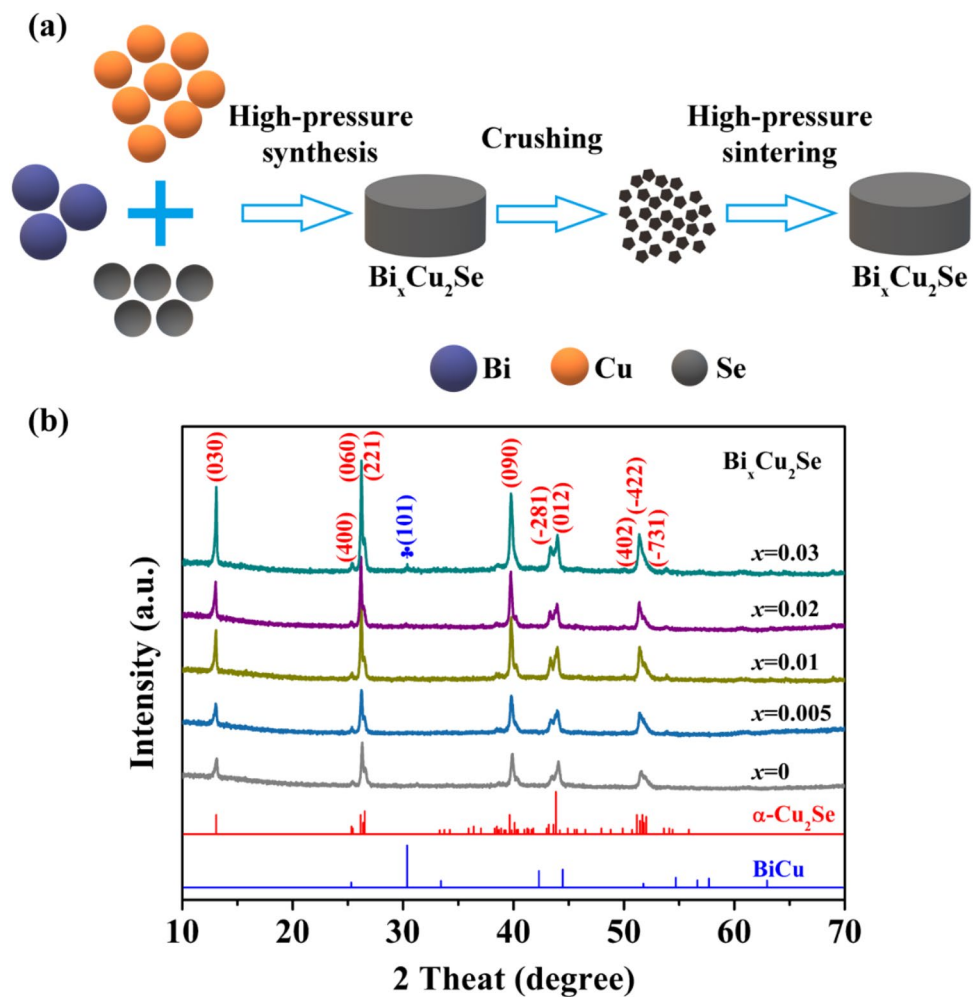
2.2 Characterization and measurement

Powder X-ray diffraction (XRD) patterns were performed on a powder diffractometer (SmartLab3KW, Rigaku) using Cu K_α ($\lambda = 1.5406 \text{ \AA}$) radiation to verify the crystal structure. The microstructures were investigated by field emission scanning electron microscopy (FESEM, ZEISS MERLIN Compact, Germany) and high-resolution transmission electron microscopy (HRTEM, Magellan-400, America). The compositions were determined by an electron probe microanalyzer (EPMA) through trace element testing. The chemical binding states of elements were analyzed by the X-ray Photoelectron Spectroscopy (XPS, Escalab 250Xi). The Seebeck coefficient and electrical resistivity measurements were conducted by the thermoelectric measurement system (ZEM-3, Ulvac-Riko, Japan) with rectangular shaped samples ($\sim 3 \times 3 \times 8 \text{ mm}^3$). The thermal conductivity was calculated by applying the formula: $\kappa = \rho C_p D$, where the thermal diffusivity coefficient (D) was measured by the laser flash method (Netzsch, LFA-467, Germany), the specific heat (C_p) was calculated by Dulong–Petit formula, and the density (ρ) was measured by the Archimedes method. The measurements were conducted in temperature range of 323 K ~ 873 K. The Hall coefficient (R_H) was measured by Hall effect measurement system (HMS-5500, ECOPIA) with a magnetic field of 0.5 T to calculate carrier concentration (n_H) and mobility (μ_H) according to the formula $n_H = 1/eR_H$ and $\mu_H = \sigma R_H$ (where e is electronic charge).

3 Results and discussions

Figure 1b shows the room-temperature XRD patterns of sintered Bi_xCu₂Se ($x=0, 0.005, 0.01, 0.02, 0.03$) samples. The XRD diffraction peaks were well matched with the α -phase Cu₂Se (PDF#27–1131). Besides, a very small amount BiCu phase (marked with blue) was detected with the increased Bi contents. The formation of BiCu could be resulted from the reaction between the extra Bi and the precipitated Cu, due to the low solubility limit of Bi in

Fig. 1 **a** Schematic of the manufacturing process of the Bi-doped Cu_2Se samples, **b** room-temperature XRD patterns of $\text{Bi}_x\text{Cu}_2\text{Se}$ samples



Cu_2Se [22] and the intrinsic Cu deficiency of Cu_2Se . The influence of BiCu phase on TE properties of Cu_2Se was not considered because of the small amount and the lack of detailed literature about BiCu material.

The morphologies of fractured surfaces for $\text{Bi}_x\text{Cu}_2\text{Se}$ bulks are shown in Fig. 2 (a–e). Overall, the layered grains densely stacked together without preferred orientation. The bulk samples exhibited grain size in the magnitude of 1–10 μm . Besides, a large number of grain particles and pores were randomly distributed on the grain surface or grain boundaries with size of 40 nm to above 1 μm . Bi doping did not cause distinct changes in the morphology of Cu_2Se , as shown in Fig. 2f. All $\text{Bi}_x\text{Cu}_2\text{Se}$ samples exhibited relative density of 97.4–98.3% (theoretical density 6.86 g/cm^3). Those abundant grain boundaries, micropores and wide distribution of grain size could play a key role in reducing lattice thermal conductivity [28–30].

Figure 3a is the energy-dispersive spectroscopy (EDS) mapping image of the $\text{Bi}_{0.005}\text{Cu}_2\text{Se}$ bulk sample after long time polishing. From the EDS results shown in Fig. 3b–d,

we can see that the elements are uniformly distributed, and no regions with enrichment are observed.

To determine the actual chemical compositions of the $\text{Bi}_x\text{Cu}_2\text{Se}$ samples, electron probe microanalysis (EPMA) were performed, as shown in Table 1. The results showed that Bi content was distinctly lower than the nominal ratio of $\text{Bi}_x\text{Cu}_2\text{Se}$ samples, which was resulted from the low-doping efficiency of Bi due to the low solubility of Bi in the Cu–Se phase diagram [31]. The above-mentioned XRD patterns were consistent with the EPMA results.

Figure 4a shows the XPS survey spectra of $\text{Bi}_{0.005}\text{Cu}_2\text{Se}$ sample, which confirms the presence of Cu 2p, Se 3d and Bi 4f energy states. The binding energies in XPS analysis are referred to C 1s peak at 284.1 eV. As shown in Fig. 4b, the Bi 4f doublet peaks appear at 160.3 and 166.0 eV with an energy split of 5.7 eV, which can be assigned to Bi^{3+} . The presence of Cu 2p_{3/2} and Cu 2p_{1/2} peaks at 932.4 eV and 952.2 eV can be attributed to Cu^+ (Fig. 4c). Besides, the low-intensity satellite peaks are distinguished, which indicates that the presence of Cu^{2+} ions. The Se 3d_{5/2} and

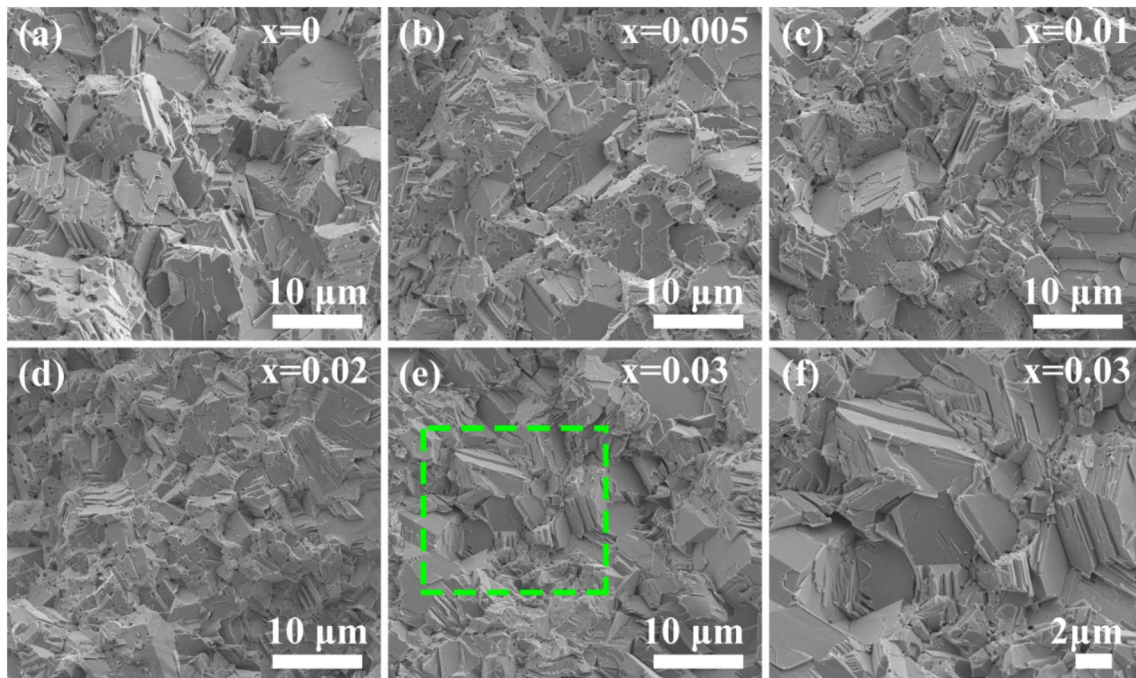
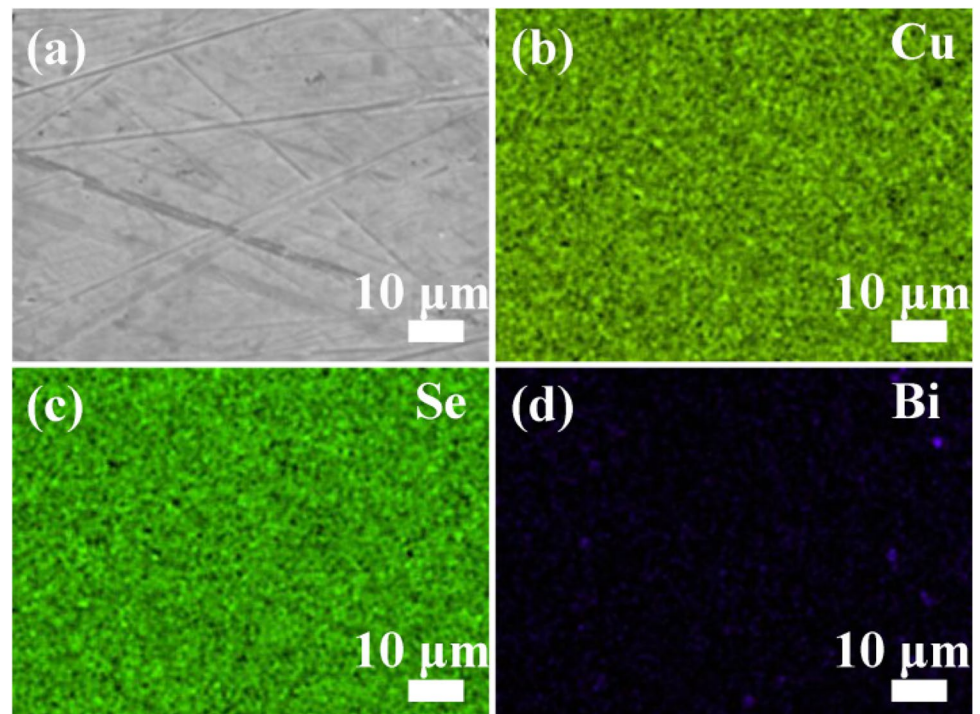


Fig. 2 a–e The typical SEM images of fractured surfaces for the Bi_xCu₂Se ($x=0, 0.005, 0.01, 0.02, 0.03$) samples, f enlarged views of the marked region in (e)

Fig. 3 a EDS mapping image of Bi_{0.005}Cu₂Se bulk sample. The distribution of energy spectrum elements of b Cu, c Se, and d Bi



Se $3d_{3/2}$ peaks at 53.9 and 54.5 eV can be attributed to Se (II) states as shown in Fig. 4d. The XPS results demonstrate that Bi is successfully doped into Cu₂Se samples.

Typical HRTEM images of Bi_{0.005}Cu₂Se sample are exhibited in Fig. 5. The calculated lattice spacings can be corresponded to the crystal planes of Cu₂Se, as shown in

Table 1 Atomic ratio of Cu, Se and Bi for Bi_xCu₂Se samples by EPMA

Nominal composition	Cu (at%)	Se (at%)	Bi (at%)	EPMA composition
Cu ₂ Se	65.02	34.98	0	Cu ₂ Se _{1.08}
Bi _{0.005} Cu ₂ Se	66.11	33.77	0.12	Bi _{0.0036} Cu ₂ Se _{1.02}
Bi _{0.01} Cu ₂ Se	66.38	33.49	0.13	Bi _{0.004} Cu ₂ Se _{1.01}
Bi _{0.02} Cu ₂ Se	66.22	33.55	0.23	Bi _{0.007} Cu ₂ Se _{1.01}
Bi _{0.03} Cu ₂ Se	66.04	33.58	0.38	Bi _{0.011} Cu ₂ Se _{1.02}

Fig. 5a and b. Exceptionally, the lattice spacing of 0.290 nm could be corresponded to crystal planes of BiCu, which is constant with XRD results. The lattice dislocations and fringes marked by white circles could effectively scatter phonons and reduce lattice thermal conductivity. Certainly, the substitution of Cu⁺ by Bi³⁺ partially would introduce point defects. These lattice defects, as well as the abundant grain boundaries, micropores and BiCu phase, can effectively enhance the phonon' scattering and reduce the lattice thermal conductivity.

Figure 6 shows electrical properties versus temperature for Bi_xCu₂Se ($x=0, 0.005, 0.01, 0.02$ and 0.03) samples in temperature range of 323–873 K. The TE properties near the phase transition temperature about 400 K were not discussed

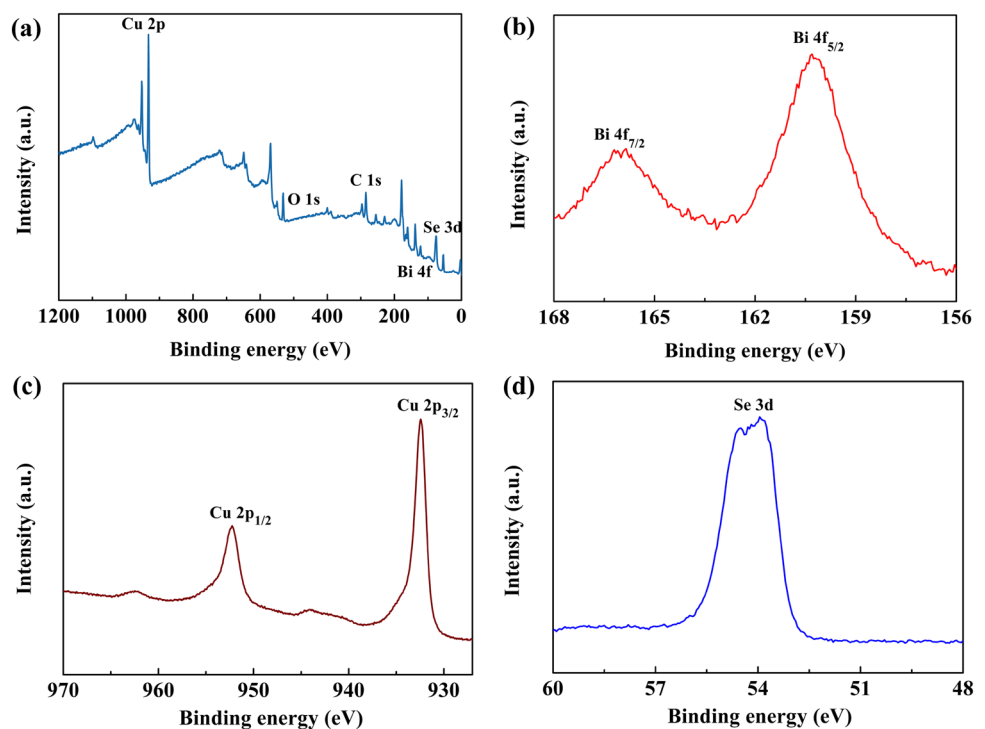
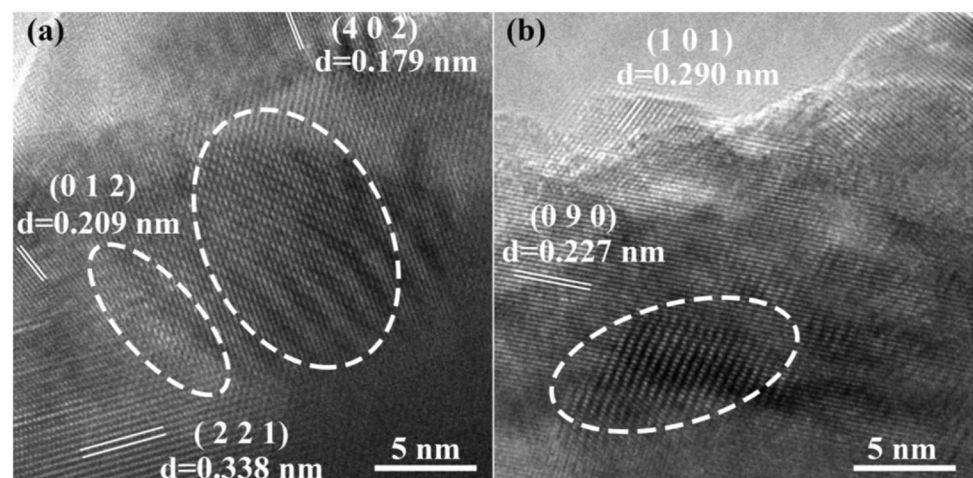
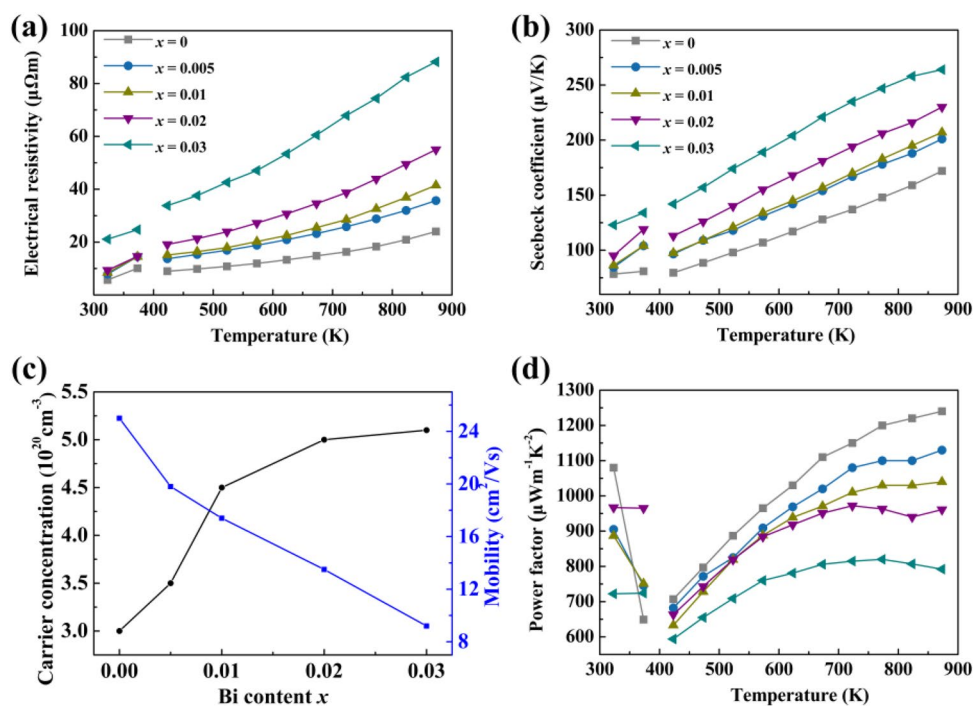
Fig. 4 a XPS spectra of Bi_{0.005}Cu₂Se sample, and high-resolution XPS spectra of b Bi, c Cu and d Se**Fig. 5** Representative HRTEM images for Bi_{0.005}Cu₂Se sample

Fig. 6 Temperature-dependent electrical properties of $\text{Bi}_x\text{Cu}_2\text{Se}$ samples. **a** Electrical resistivity, **b** Seebeck coefficient, **c** carrier concentration and mobility, and **d** power factor



below, due to the occurrence of discontinuity. However, the TE properties of high-temperature β -phase Cu_2Se were analyzed in detail. The electrical resistivity increased with the increasing measured temperature (Fig. 6a), suggesting a typical degenerated semiconductor character. The positive Seebeck coefficients in Fig. 6b indicated the P-type conducting behavior with holes as main carriers, due to the existence of Cu vacancies in Cu_2Se [32]. Both the electrical resistivity and Seebeck coefficient increased with the increasing Bi contents.

The carrier concentration and mobility at room temperature of $\text{Bi}_x\text{Cu}_2\text{Se}$ samples were measured, as shown in Fig. 6c. With the increasing Bi contents, the carrier concentration increased and the carrier mobility decreased. The hole carrier concentration n_{H} at room temperature for $\text{Bi}_{0.03}\text{Cu}_2\text{Se}$ is $5.1 \times 10^{20} \text{ cm}^{-3}$, which is 70% higher than that of pure Cu_2Se , suggesting that large amount Cu vacancies exist in the sample. It might be derived from the decreased strengthen of the bonding energy by the increased Bi–Se bond length ($\sim 2.81 \text{ \AA}$) compared to Cu–Se bond length ($\sim 2.46 \text{ \AA}$), which could increase vacancies and thus increase hole concentration. Such significant increase in carrier concentration of doped samples can lead to reduced carrier mobility. In addition, the BiCu phase and microstructures can also affect electrical properties [33–35], although their effects on electrical properties cannot be quantified.

The power factor values were calculated according to $\text{PF} = S^2/\rho$, as shown in Fig. 6d. The maximum power factor value was up to $1240 \mu\text{Wm}^{-1} \text{ K}^{-2}$ for pristine Cu_2Se . The power factor values for Bi-doped Cu_2Se decreased with

increasing Bi contents. Although the power factors of Bi-doped Cu_2Se samples were deteriorated compared with the pure Cu_2Se , it is still worth investigating due to the relatively low thermal conductivity.

Figure 7a shows the temperature dependence of thermal conductivity for $\text{Bi}_x\text{Cu}_2\text{Se}$ samples. The relatively low thermal conductivity (κ) for pure Cu_2Se was below $0.87 \text{ Wm}^{-1} \text{ K}^{-1}$ in the whole temperature range due to the superionic conductor behavior. The $\text{Bi}_{0.01}\text{Cu}_2\text{Se}$ sample obtained the lowest thermal conductivity of $0.58 \text{ Wm}^{-1} \text{ K}^{-1}$, which is approximately a 33.3% reduction than that of pure Cu_2Se at 873 K. Figure 7b shows the temperature-dependent lattice thermal conductivity (κ_{l}) for $\text{Bi}_x\text{Cu}_2\text{Se}$ bulk samples. The κ_{l} was obtained by subtracting the carrier thermal conductivity (κ_{c}) from κ , where κ_{c} can be calculated using the Wiedemann–Franz law, $\kappa_{\text{c}} = L_0\sigma T$, where $L_0 = 1.5 \times 10^{-8} \text{ V}^2 \text{ K}^{-2}$. The κ_{l} increased with increasing Bi content, which may be attributed to the doping mechanism of heavy metal cations. Compared with Cu^+ ions, Bi^{3+} ions have a larger atomic mass and radius, which can prevent the propagation of phonons and limit the diffusion of Cu^+ ions. Therefore, Bi doping reduced the degree of disorder of Cu^+ ions, weakened phonon scattering, and led to an increase in lattice thermal conductivity [8, 15]. Due to the carrier thermal conductivity greatly reduced after Bi doping, the total thermal conductivities of the Bi-doped samples were lower than that of pure Cu_2Se .

The temperature dependence of zT values is calculated as shown in Fig. 7c. Eventually, $\text{Bi}_{0.005}\text{Cu}_2\text{Se}$ sample achieved the highest zT of 1.57 at 873 K, which was 25% higher than

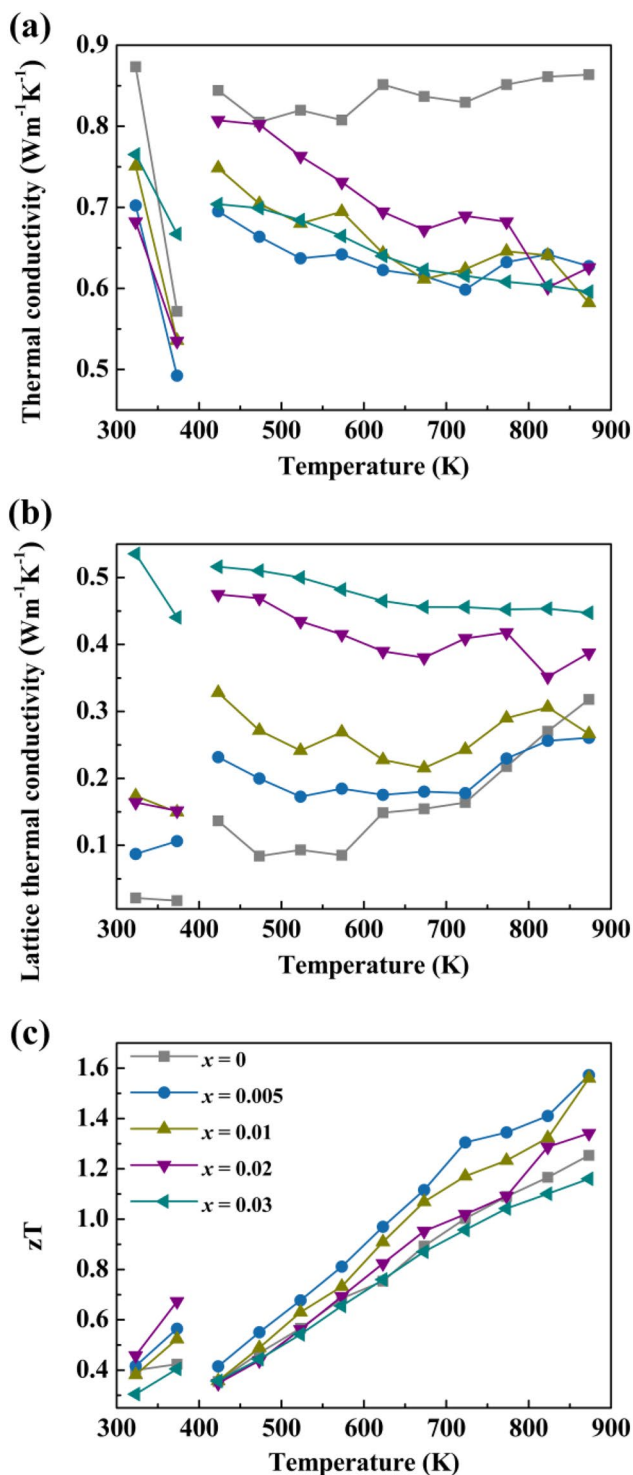


Fig. 7 Temperature-dependent thermoelectric properties of Bi_xCu₂Se samples. **a** Thermal conductivity, **b** lattice thermal conductivity and **c** zT value

that of pristine Cu₂Se (zT = 1.25 at 873 K). For Cu₂Se system, the introducing of Bi regulated carrier concentration and the complexity of the system, resulting in the higher zT. The zT values of Bi_xCu₂Se (x = 0.005, 0.01, 0.02) samples

by high-pressure synthesis in this work were 0.56, 0.52 and 0.67 at 373 K, respectively, which were higher than the zT value of 0.43 at 373 K obtained for Cu_{1.982}Bi_{0.006}Se in reference [22]. Therefore, the carrier concentration and thermal conductivity can be optimized to achieve high-TE performance by heavy-elements doping and high-pressure technology.

4 Conclusion

In summary, the high-pressure and high-temperature technology was adopted to effectively suppress the segregation of Cu and Se elements, and the polycrystalline Bi_xCu₂Se (x = 0, 0.005, 0.01, 0.02, 0.03) samples were successfully fabricated. Bi_xCu₂Se compounds existed as a monoclinic α-Cu₂Se phase at room temperature, while BiCu phase was detected in Bi_xCu₂Se (x > 0) samples due to the low solubility limit. The resistivity and Seebeck coefficient of Bi_xCu₂Se samples increased with the increasing Bi contents, and the power factor gradually decreased. Bi doping generated an increased carrier concentration and decreased carrier mobility. The disorder degree of Cu⁺ ions was reduced by Bi doping, which weakened the phonon scattering and then enhanced the lattice thermal conductivity, but the total thermal conductivities of the Bi-doped samples were significantly reduced. As a result, Bi_{0.005}Cu₂Se sample obtained a maximum zT of 1.57 at 873 K, which was 25% higher than that of pristine Cu₂Se (zT ~ 1.25). This work provides a guidance for further research of heavy-element doping in liquid-like thermoelectric materials.

Acknowledgements This work was supported by the National Natural Science Foundation of China (No. 11704340 and 11804305), the Key Research Project of Higher Education Institution of Henan Province (No. 19A140006) and the Key Project for Science and Technology Development of Henan Province (No. 192102210158).

References

1. X.L. Shi, J. Zou, Z.G. Chen, Advanced thermoelectric design: from materials and structures to devices. *Chem. Rev.* **120**(15), 7399–7515 (2020)
2. K. Zhao, P. Qiu, X. Shi, L. Chen, Recent advances in liquid-like thermoelectric materials. *Adv. Funct. Mater.* **30**(8), 1903867 (2020)
3. Y. Wang, L. Yang, X.L. Shi, X. Shi, L. Chen, M.S. Dargusch, J. Zou, Z.G. Chen, Flexible thermoelectric materials and generators: challenges and innovations. *Adv. Mater.* **31**(29), 1807916 (2019)
4. M. Shen, S. Lu, Z. Zhang, H. Liu, W. Shen, C. Fang, Q. Wang, L. Chen, Y. Zhang, X. Jia, Bi and Sn co-doping enhanced thermoelectric properties of Cu₃SbS₄ materials with excellent thermal stability. *ACS Appl. Mater. Interfaces* **12**(7), 8271–8279 (2020)
5. M. Hong, W.Y. Lyv, M. Li, S.D. Xu, Q. Sun, J. Zou, Z.G. Chen, Rashba effect maximizes thermoelectric performance of GeTe derivatives. *Joule* **4**(9), 2030–2043 (2020)

6. S. Zhang, X.M. Zhang, S.Q. Hao, X. Hua, P.B. Trevor, U. Ctirad, W. Chris, P.D. Vinayak, G.K. Mercouri, Dual alloying strategy to achieve a high thermoelectric figure of merit and lattice hardening in p-Type nanostructured PbTe. *ACS Energy Lett.* **3**(10), 2593–2601 (2018)
7. L.D. Zhao, S.H. Lo, Y.S. Zhang, H. Sun, G.J. Tan, U. Ctirad, C. Wolverton, P.D. Vinayak, G.K. Mercouri, Ultralow thermal conductivity and high thermoelectric figure of merit in SnSe crystals. *Nature* **508**(7496), 373–377 (2014)
8. H.L. Liu, X. Shi, F.F. Xu, L.L. Zhang, W.Q. Zhang, L.D. Chen, Q. Li, U. Ctirad, D. Tristan, G.J. Snyder, Copper ion liquid-like thermoelectrics. *Nat. Mater.* **11**, 422–425 (2012)
9. G. Lubomir, D. Marek, S. Oksana, P. Adam, Crystal structure of Cu₂Se. *Chem. Met. Alloys* **4**, 200–205 (2011)
10. A.L.N. Stevels, F. Jellinek, Phase transformations in copper chalcogenides: I. The copper–selenium system. *RECUEIL* **90**(3), 273–283 (1971)
11. R. Nunna, P.F. Qiu, M.J. Yin, H.Y. Chen, R. Hanus, Q.F. Song, T.S. Zhang, M.Y. Chou, T.A. Matthias, J.Q. He, G.J. Snyder, X. Shi, L.D. Chen, Ultrahigh thermoelectric performance in Cu₂Se-based hybrid materials with highly dispersed molecular CNTs. *Energy Environ. Sci.* **10**, 1928–1953 (2017)
12. A.A. Olvera, N.A. Moroz, P. Sahoo, P. Ren, T.P. Bailey, A.A. Page, C. Uher, P.F.P. Poudeu, Partial indium solubility induces chemical stability and colossal thermoelectric figure of merit in Cu₂Se. *Energy Environ. Sci.* **10**, 1668–1676 (2017)
13. J. Pei, L.J. Zhang, B.P. Zhang, P.P. Shang, Y.C. Liu, Enhancing the thermoelectric performance of Ce_xBi₂S₃ by optimizing the carrier concentration combined with band engineering. *J. Mater. Chem. C* **5**, 12492–12499 (2017)
14. C. Joseph, C.B. Hans, Effect of point imperfections on lattice thermal conductivity. *Phys. Rev.* **120**(4), 1149 (1960)
15. W.D. Liu, X.L. Shi, M. Hong, L. Yang, R. Moshwan, Z.G. Chen, J. Zou, Ag doping induced abnormal lattice thermal conductivity in Cu₂Se. *J. Mater. Chem. C* **6**, 13225–13231 (2018)
16. Q.J. Hu, Z. Zhu, Y.W. Zhang, X.J. Li, H.Z. Song, Y.J. Zhang, Remarkably high thermoelectric performance of Cu_{2-x}Li_xSe bulks with nanopores. *J. Mater. Chem. A* **6**, 23417–23424 (2018)
17. Y.S. Jin, M.K. Han, S.J. Kim, Na-doping effects on thermoelectric properties of Cu_{2-x}Se nanoplates. *Appl. Sci.* **8**(1), 12 (2018)
18. K.P. Zhao, A.B. Blichfeld, H.Y. Chen, Q.F. Song, T.S. Zhang, C.X. Zhu, D.D. Ren, R. Hanus, P.F. Qiu, B.B. Iversen, F.F. Xu, G.J. Snyder, X. Shi, L.D. Chen, Enhanced thermoelectric performance through tuning bonding energy in Cu₂Se_{1-x}S_x liquid-like materials. *Chem. Mater.* **29**, 6367–6377 (2017)
19. T.P. Bailey, S. Hui, H.Y. Xie, A. Olvera, P.F.P. Poudeu, X.F. Tang, U. Ctirad, Enhanced ZT and attempts to chemically stabilize Cu₂Se via Sn doping. *J. Mater. Chem. A* **4**, 17225–17235 (2016)
20. K.P. Zhao, M.J. Guan, P.F. Qiu, A.B. Blichfeld, E. Eikeland, C.X. Zhu, D.D. Ren, F.F. Xu, B.B. Iversen, X. Shi, L.D. Chen, Thermoelectric properties of Cu₂Se_{1-x}Te_x solid solutions. *J. Mater. Chem. A* **6**, 6977–6986 (2018)
21. J.D. Lei, Z. Ma, D. Zhang, Y.Q. Chen, C. Wang, X.Y. Yang, Z.X. Cheng, Y.X. Wang, High thermoelectric performance in Cu₂Se superionic conductor with enhanced liquid-like behaviour by dispersing SiC. *J. Mater. Chem. A* **7**, 7006–7014 (2019)
22. W.W. Liao, L. Yang, J. Chen, D.L. Zhou, X.L. Qu, K. Zheng, G. Han, J.B. Zhou, M. Hong, Z.G. Chen, Realizing Bi-doped α-Cu₂Se as a promising near-room-temperature thermoelectric material. *Chem. Eng. J.* **371**, 593–599 (2019)
23. Y.W. Zhang, X.P. Jia, L. Deng, X. Guo, H.R. Sun, B. Sun, B.W. Liu, H.A. Ma, Evolution of thermoelectric properties and anisotropic features of Bi₂Te₃ prepared by high pressure and high temperature. *J. Alloys Compd.* **632**, 514–519 (2015)
24. T.C. Su, X.P. Jia, H.A. Ma, J.G. Guo, Y.P. Jiang, N. Dong, L. Deng, X.B. Zhao, T.J. Zhu, C. Wei, Thermoelectric properties of nonstoichiometric PbTe prepared by HPHT. *J. Alloys Compd.* **468**, 410–413 (2009)
25. Y.W. Zhang, X.P. Jia, H.R. Sun, B. Sun, B.W. Liu, H.Q. Liu, L.J. Kong, H.A. Ma, *J. Alloys Compd.* **667**, 123–129 (2016)
26. L.S. Xue, Z.F. Zhang, W.X. Shen, H.A. Ma, Y.W. Zhang, C. Fang, X.P. Jia, Thermoelectric performance of Cu₂Se bulk materials by high-temperature and high-pressure synthesis. *J. Materiomics* **5**, 103–110 (2019)
27. L.S. Xue, W.X. Shen, Z.F. Zhang, M.J. Shen, W.T. Ji, C. Fang, Y.W. Zhang, X.P. Jia, Off-stoichiometry effects on the thermoelectric properties of Cu_{2+δ}Se (-0.1 ≤ δ ≤ 0.05) compounds synthesized by high-pressure and high-temperature method. *CrystEngComm* **22**, 695–700 (2020)
28. Y. Nakamura, M. Isogawa, T. Ueda, S. Yamasaka, H. Matsui, J. Kikkawa, S. Ikeuchi, T. Oyake, T. Hori, J. Shiomi, A. Sakai, Anomalous reduction of thermal conductivity in coherent nanocrystal architecture for silicon thermoelectric material. *Nano Energy* **12**, 845–851 (2015)
29. S. Yamasaka, Y. Nakamura, T. Ueda, S. Takeuchi, A. Sakai, Phonon transport control by nanoarchitecture including epitaxial Ge nanodots for Si-based thermoelectric materials. *Sci. Rep.* **5**, 14490 (2015)
30. M. Linu, P. Anil, O. Dotun, J. Ericmoore, R. Jayangani, S. Barbara, B. Lukas, S. Jerzy, Atomistic and experimental study on thermal conductivity of bulk and porous cerium dioxide. *Sci. Rep.* **9**, 6326 (2019)
31. N.B. Babanly, Y.A. Yusibov, Z.S. Aliev, M.B. Babanly, Phase equilibria in the Cu–Bi–Se system and thermodynamic properties of copper selenobismuthates. *Russ. J. Inorg. Chem.* **55**(9), 1471–1481 (2010)
32. W.D. Tristan, S.W. Kai, G.Z. Wolfgang, B.R. Chen, L.M. Stephanie, W. Ulrike, P.J. Klaus, P. Martin, J.B. Michael, G.J. Snyder, T. Wolfgang, Influence of compensating defect formation on the doping efficiency and thermoelectric properties of Cu_{2-y}Se_{1-x}Br_x. *Chem. Mater.* **27**, 7018–7027 (2015)
33. J.P. Heremans, C.M. Jaworski, Experimental study of the thermoelectric power factor enhancement in composites. *Appl. Phys. Lett.* **93**(12), 122107 (2008)
34. A. Shakouri, Recent developments in semiconductor thermoelectric physics and materials. *Annu. Rev. Mater. Res.* **41**, 399–431 (2011)
35. A.M. Dehkordi, M. Zebarjadi, J. He, T.M. Tritt, Thermoelectric power factor: enhancement mechanisms and strategies for higher performance thermoelectric materials. *Mater. Sci. Eng. R* **97**, 1–22 (2015)

Publisher's Note Springer Nature remains neutral with regard to jurisdictional claims in published maps and institutional affiliations.